**Annales
Geophysicae**

Similarities and differences in polar mesosphere summer echoes observed in the Arctic and Antarctica

R. Latteck[1]**, W. Singer**[1]**, R. J. Morris**[2]**, W. K. Hocking**[3]**, D. J. Murphy**[2]**, D. A. Holdsworth**[2,4]**, and N. Swarnalingam**[3]

[1]Leibniz-Institut für Atmosphärenphysik, Kühlungsborn, Germany
[2]Australian Antarctic Division, Kingston,Tasmania, Australia
[3]University of Western Ontario, London, Ontario, Canada
[4]Atmospheric Radar Systems, Thebarton, South Australia, Australia

Abstract. Polar Mesosphere Summer Echoes (PMSE) have been observed in the high latitudes of the Northern and Southern Hemisphere for several years using VHF radars located at Andenes/Norway (69° N, 16° E), Resolute Bay/Canada (75° N, 95° W), and Davis/Antarctica (69° S, 78° E). The VHF radars at the three sites were calibrated using the same methods (noise source and delayed transmitting signal) and identical equipment. Volume reflectivity was derived from the calibrated echo power and the characteristics of the seasonal variation of PMSE were estimated at the sites for the years 2004 to 2007. The largest peak volume reflectivity of about 2×10^{-9} m^{-1} was observed at Andenes compared with their counterparts at Davis ($\sim 4 \times 10^{-11}$ m^{-1}) and Resolute Bay ($\sim 6 \times 10^{-12}$ m^{-1}). The peak of the PMSE height distribution is 85.6 km at Davis which is about 1 km higher than at Andenes. At Resolute Bay the height distribution peaks at about 85 km but only a few layers were found below 84 km. The mean PMSE occurrence rate is 83% at Andenes, 38% at Davis with larger variability and only 18% at Resolute Bay (in late summer). The duration of the PMSE season varies at Andenes from 104 to 113 days and at Davis from 88 to 93 days. In general the PMSE seasons starts about 5 days later at Davis and ends about 10 days earlier compared to Andenes. In all three seasons the PMSE occurrence suddenly drops to a much lower level at Davis about 32 days after solstice whereas the PMSE season decays smoothly at Andenes. The duration of the PMSE season at Andenes and Davis is highly correlated with the presence of equatorward directed winds, the observed differences in PMSE occurrence are related to the mesospheric temperatures at both sites.

1 Introduction

Polar mesosphere summer echoes (PMSE) are strong enhancements of signal power at very high radar frequencies that occur between about 80 and 95 km in altitude at polar and middle latitudes during summer. An example of such an echo represented by the received relative signal power is shown in Fig. 1. The phenomenon of strong radar echoes from the mesopause region during summer is well known from VHF radar observations at polar latitudes in the Northern Hemisphere (NH) for more than 20 years. PMSE are caused by inhomogeneities in the electron density of the radar Bragg scale within the plasma in the cold summer mesopause region (see Kelley et al., 1987). The first mesospheric summer echoes were actually observed with the SOUSY radar (53.5 MHz) in the Harz mountains of Germany (52° N) by Czechowsky et al. (1979) before the first echoes of this type were seen at the polar latitude site Poker Flat by Ecklund and Balsley (1981). A detailed review can be found in Cho and Röttger (1997). An overview on the current understanding of this phenomenon has recently been published by Rapp and Lübken (2004).

Appropriate measurements in the Southern Hemisphere (SH), however were rare in the past and limited to low southern latitudes basically due to the lack of radars deployed in the southern polar region. First experiments for PMSE observations in the Southern Hemisphere were carried out by Balsley et al. (1993) at Machu Picchu located on King George Island (62.1° S) in the austral summer of 1992/1993. The
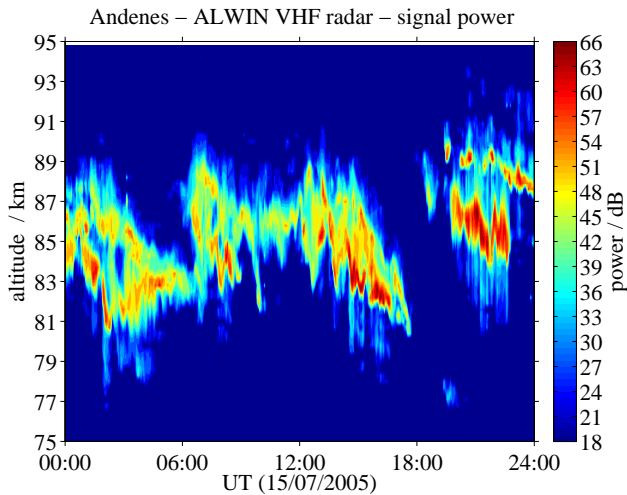
Andenes – ALWIN VHF radar – signal power

Fig. 1. Relative signal power of Polar Mesosphere Summer Echoes observed on 15 July 2005 with the ALWIN MST radar at Andenes.

analysis of these observations led to the conclusion that there are no PMSE at this latitude (Balsley et al., 1993) or, if they exist at all, these echoes had to be at least 34 to 44 dB weaker than their NH counterparts (Balsley et al., 1995). One year later the first SH PMSE were observed with the improved radar at Machu Picchu (Woodman et al., 1999). This observation reinforced previous conclusions that there are large differences between the strength of PMSE observed in the two hemispheres. Woodman et al. (1999) attributed this asymmetry to differences in mesopause temperature between the two sites. Huaman and Balsley (1999) suggested that differences in water vapour and dynamics might be the cause of the observed lag in PMSE occurrence. However, Lübken et al. (1999) showed on the basis of in situ measurements that there is no significant difference in the polar mesopause temperature between both hemispheres.

Morris et al. (2004) presented the first morphology of daily and seasonal occurrence of SH-PMSE based on VHF radar observation at Davis during austral summer of 2003/2004. They concluded that SH PMSE observed at 68.6° S exhibit similar characteristics to published observations (i.e. altitude, intensity, diurnal and seasonal occurrence distributions) at similar northern latitudes, at least for the last three weeks of the austral PMSE season. Latteck et al. (2007) performed the first comparison of continuous measurements of PMSE collected at Andenes (69° N) during the boreal summer of 2004 and Davis (69° S) during the austral summer of 2004/2005 on the basis of radar volume reflectivity. They found that PMSE observed at Davis are less reflective and reach maximum heights of about 1 km higher than those in the Northern Hemisphere at an equivalent latitude near 69°. Furthermore, PMSE occurred less frequently but with greater variability above Davis. The studied PMSE seasons started

at Andenes and Davis around 34 days before solstice but the duration of the PMSE season was about 9 days shorter at Davis. Kirkwood et al. (2007) compared PMSE which were obtained with cross-calibrated VHF radars in the Arctic (Kiruna, 68° N) and Antarctica (Wasa, 73° S) and found very similar PMSE characteristics between the two sites for the late summer season. Hence the interhemispheric and latitudinal differences of the appearance and intensity of PMSE still remains an open question and the use of system independent parameters for the comparison of PMSE from different sites is necessary. In the present study the inter-annual variability of PMSE occurrence in the Northern and Southern Hemisphere has been studied incorporating two additional years of PMSE observations at Davis and Andenes, together with PMSE observations at the polar cap site at Resolute Bay.

Radar volume reflectivity η is a system independent parameter in contrast to, e.g., relative signal strength or signal-to-noise ratio which depend on the individual radar characteristics (e.g. transmitting power, antenna gain, and receiver band width) and the experiment configurations (e.g. coherent integrations, code length, and pulse width). Radar volume reflectivity is defined as the power which would be scattered if all powers were scattered isotropically with a power density equal to that of the backscattered radiation, per unit volume and per unit incident power density (Hocking, 1985). It can be expressed as

$$\eta = \frac{P_r \, 128 \, \pi^2 \, 2 \ln(2) \, r^2}{P_t \, G_t \, G_r \lambda^2 \, e \, \theta_{[1/2]}^2 \, c \, \tau} \tag{1}$$

where r is the range to the scatterers, G_t and G_r are the one-way gain of the transmitting and receiving antenna respectively, $\theta_{[1/2]}$ is the one-way half power half-width of the transmitting antenna beam, λ is the radar wavelength, e is the system efficiency containing mainly the losses of the antenna feeding system, P_t is the transmitted peak power, P_r is the received signal power, c is the speed of light, and τ is the effective pulse width (Hocking and Röttger, 1997). The factor $2 \ln(2)$ is a correction term related to the non-uniform antenna gain over the half-power beam-width (Probert-Jones, 1962).

The system dependent parameters of Eq. (1) can be combined into a system factor c_{sys}, so finally the radar reflectivity η depends only on the range to the scatterers r and the absolute value of the received signal power P_r.

$$\eta = P_r \cdot c_{sys} \cdot r^2 \tag{2}$$

The correct determination of the received signal power requires the calibration of the radar system. Two different radar calibration methods are presented in Sect. 2.

2 Calibration of the radar receiving system

The receiving system of an atmospheric radar usually archives the received signal power in arbitrary units (au)
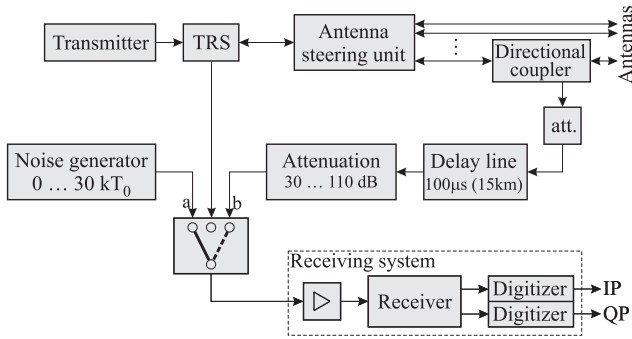
Fig. 2. Principle of radar calibration using **(a)** a calibrated noise source, and **(b)** the delayed and attenuated transmitted signal.

Fig. 3. Calibration with a noise source: noise power in arbitrary units vs. noise temperature. The red circle represents the receiver noise temperature.

dependent on the resolution of the A/D converter. These values furthermore depend on the receiver characteristics (e.g. gain and bandwidth) as well as on experiment configurations (e.g. coherent integrations and the transmitted wave form). In order to get the received signal power P_r in units of a physical quantity the relation between the stored digital values and the physical quantity has to be estimated. This procedure is commonly called "absolute calibration" and methods are described in various papers (e.g. Green et al., 1983; Inhester et al., 1990).

A common calibration method for MST radars uses the background noise detected from running standard experiments and the derived signal-to-noise ratio for estimation of the received echo power. The radio noise at VHF frequencies is mostly of extra-terrestrial/cosmic origin and undergoes a daily variation which depends on the radar frequency and the beam pointing direction. Maps of the cosmic noise temperature are available but difficult to use as these maps are often not available for the radar operation frequency. These maps have to be converted into equivalent cosmic noise temperatures at the radar operation frequency using assumptions about the frequency dependence of the cosmic noise temperature. In addition, the sampled radar data are sometimes contaminated by interfering signals or anomalous ionospheric absorption in the case of precipitation of energetic particles at high latitudes. These effects are sporadic and have to be carefully removed.

A reliable calibration of VHF radars can be achieved with a calibrated noise source fed directly into the receiving system consisting of a front end amplifier, baseband receiver and digitizer (see Sect. 2.1). Alternatively the transmitted signal itself can be used (see Sect. 2.2). The principle setup of both methods are sketched in Fig. 2.
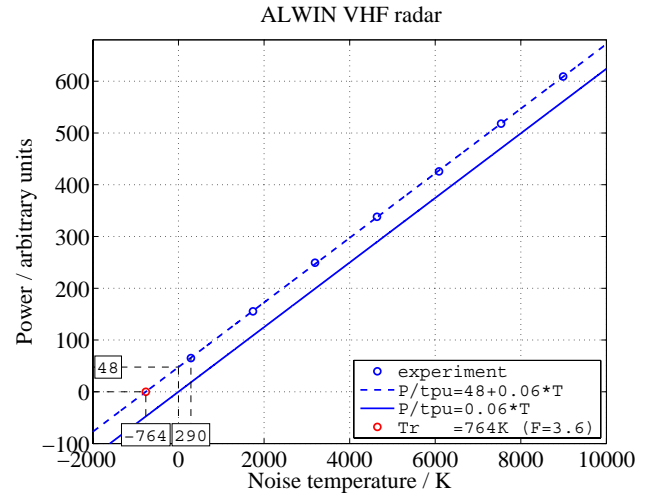
2.1 Calibration with calibrated noise source

The noise power fed into a receiver can be described by its equivalent noise temperature $T_{n.inp}$

$$P_{n.inp} = k_B B_N T_{n.inp}$$
$$= c\, T_{n.inp} \tag{3}$$

where k_B is the Boltzmann constant and B_N is the equivalent receiver noise bandwidth (Skolnik, 1990).

The relation between the inserted noise signal $P_{n.inp}$ and the noise power $P_{n.out}$ measured at the receiver output is linear with an offset for $T_{n.inp}=0$ caused by the receiver noise temperature T_r

$$P_{n.out} = g_r k_B B_N (T_r + T_{n.inp})$$
$$= a + b\, T_{n.inp} \tag{4}$$

where g_r is the overall available gain of the receiving system.

Figure 3 shows this relation for different noise temperature levels as used for the ALWIN VHF radar calibration.

The analyzed data are typically stored in arbitrary units (au). It is possible to convert each stored noise power from digital units directly into its equivalent noise temperature using the estimated parameters offset a and slope b.

$$T_{n.inp} = \frac{P_{n.out}[au] - a}{b} \tag{5}$$

Furthermore a substitution of $T_{n.inp}$ in Eq. (3) with Eq. (5) leads to a calibration factor c_n for incoherent detected signals as noise.

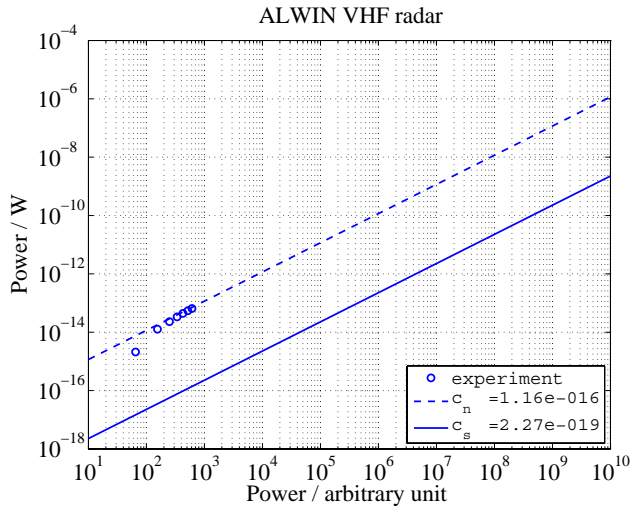$$c_n = \frac{c}{b} = \frac{P_{n.inp}[W]}{P_{n.out}[au] - a} \tag{6}$$

Fig. 4. Calibration with a noise source: signal power in physical units (Watt) vs. signal power in arbitrary units (circles and dashed line). Calibration curve (solid line) for coherent atmospheric echoes based on 16 bit coded transmit pulses and integrated by a factor of 32 during reception.

Taking into account that the use of coded pulses of length n as well as the use of m coherent integrations improve the signal-to-noise ratio by the factor of $n \cdot m$ if signals from coherent atmospheric scatterers are received, the calibration term c_n can also be used to directly convert the stored signal values from digital units into signal power.

$$
\begin{aligned}
P_{s.\text{inp}}[W] &= P_{s.\text{out}}[au] \, \frac{c_n}{n \cdot m} \\
&= P_{s.\text{out}}[au] \, c_s
\end{aligned}
\tag{7}
$$

Figure 4 shows the relation between noise power and the corresponding values in arbitrary units (circles and dashed line) after the ALWIN receiver calibration with a calibrated noise source for input powers between about 10^{-14} and 10^{-13} W. The solid line represents the calibration curve for coherent atmospheric echoes based on 16 bit coded transmit pulses and integrated by a factor of 32 during reception.

2.2 Calibration with delay line

Using the setup b shown in Fig. 2 leads directly to the calibration factor c_s for coherently received signals. The transmitted signal is taken from the antenna port using a directional coupler, delayed by some microseconds and fed into the receiver input port. The delay allows the transmitted signal to be used directly as an ideal echo whose amplitude or power can be measured at the output of the directional coupler. Since the necessary delay for a VHF radar is in the order of some 10th of a microsecond, it cannot be achieved by cable. We used an ultra-sonic delay line and obtained a delay of $100 \, \mu$s corresponding to 15 km at 53.5 MHz. Sending pulses with differ-
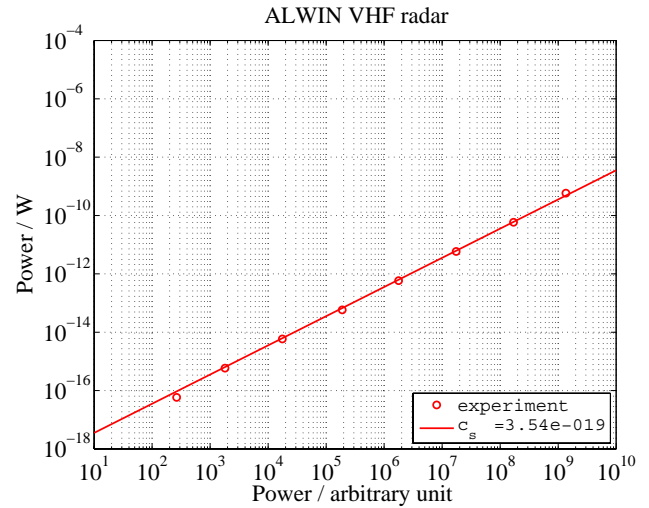

Fig. 5. Calibration with an ultra-sonic delay line: signal power in physical units (Watt) vs. signal power in arbitrary units (au) for coherent received signals.

ent amplitudes through the delay line into the receiver results in a relation shown by the circles in Fig. 5. The calibration factor c_s for coherent received signals can directly be determined from the slope of a linear fit (solid line) through these values.

$$
c_s = \frac{P_{s.\text{inp}}[W]}{P_{s.\text{out}}[au]}
\tag{8}
$$

Additionally the delay line measurements provide a precise range calibration with an accuracy better than half a range gate.

3 System parameters and experiment setups

The 53.5-MHz radar ALWIN at Andenes (69.3° N, 16.0° E) commenced operation in October 1998 (Latteck et al., 1999). The 55-MHz radar at Davis, Antarctica (68.6° S, 78.0° E) was installed late in the austral summer of 2002/2003 (Morris et al., 2004). Both radars are comparable in their basic characteristics as well as radar wavelength and antenna systems. The 51.5-MHz radar at Resolute Bay began full-time unattended operation in April 1998 (Hocking et al., 2001). A detailed description of the radars can be found in the corresponding references. The basic system parameters and experiment configurations used for PMSE observations and the resulting system factors c_{sys} of Eq. (2) are summarized in Table 1. The transmitted peak power and the system efficiency were obtained from measurements. The gain of both the transmitting and receiving antenna arrays as well as the antenna beam width (full-width at half-power) were obtained from model simulations. The Numerical Electromagnetics Code (NEC) with the Norton-Sommerfeld approximation

Table 1. Basic system parameters and experiment parameters of the VHF radars at Davis ([a]) before 24 January 2005, ([b]) since September 2005, ([c]) since November 2005, ([d]) since October 2006, at Andenes ([e]) in 2004, ([f]) since 2005, and at Resolute Bay used for PMSE observation.

Radar site	Andenes	Davis	Resolute
Latitude	69° N	69° S	75° N
Longitude	16° E	78° E	95° W
System parameters			
Radar wavelength [m]	5.6	5.5	5.8
Peak power [kW]	36	20[a]	12
		36[b]	
		41[c]	
		49[d]	
Beam width (HPFW)	6°	6°	4°
Tx antenna gain [dBi]	28.3	28.9	24.0
SA antenna gain [dBi]	20.6	21.0	–
System efficiency	0.6	0.5	0.12
Effective pulse width [m]	300	600[a]	750
		450[b]	
SA system factor c_{sys}	2.1e-08	1.9e-08[a]	
		1.4e-08[b]	
		1.2e-08[c]	
		1.0e-08[d]	
DBS system factor c_{sys}	3.6e-08	3.1e-09[a]	3.1e-07
		2.3e-09[b]	
		2.0e-09[c]	
		1.6e-09[d]	
Experiment parameters			
Coherent integrations	32[e]	116[a]	16
	64[f]	104[b]	
Number of sub pulses	16	1[a]	1
		8[b]	
Receiver gain [dB]	101	81	116
Receiver bandwidth [kHz]	500	368[a]	140
		280[b]	

was used, making allowance for the imperfect ground at the locations.

The three VHF radars at Andenes/Norway, Davis/Antarctica and Resolute Bay/Canada were calibrated using both methods as described in Sect. 2 with the same ultrasonic delay line and identical noise generators. The ALWIN VHF radar is calibrated annually, the Davis VHF radar was calibrated before and after a major system upgrade on 22 January 2005, and the Resolute Bay VHF radar was calibrated in summer 2004. The calibration results obtained with the delay line and the calibrated noise generator agree well for uncoded (single pulse) transmitted wave forms, but differences were observed for coded signals. As the delay line calibration includes all losses due to imperfect
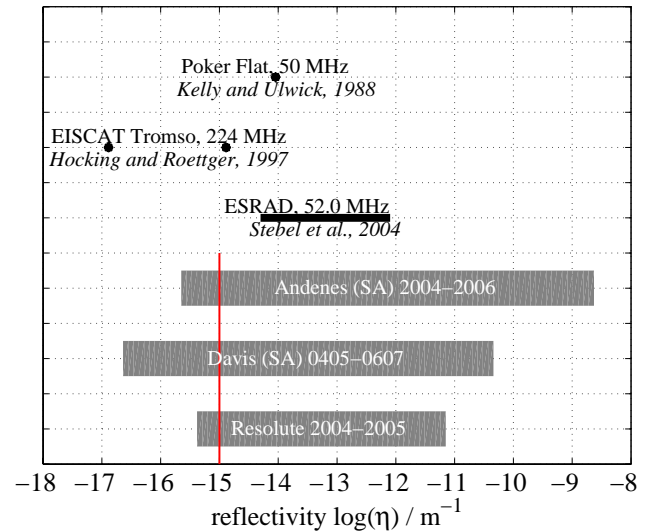

Fig. 6. Volume reflectivities detected by various VHF radars at different sites (Kelley and Ulwick, 1988; Hocking and Röttger, 1997; Stebel et al., 2004). The red line indicates the lower threshold chosen for the comparison of occurrence rates.

signal generation or decoding on reception, the calibration factor c_s obtained with this method was finally used for the determination of total received signal power with this study.

4 Results and discussion

4.1 Minimum detection limits

The occurrence of PMSE in the Northern and Southern Hemisphere (NH/SH) were studied using continuous PMSE observations during the arctic summers of 2004, 2005 and 2006 at Andenes, parts of the arctic summers of 2004 and 2005 at Resolute Bay, and the antarctic summers of 2004/2005, 2005/2006 and 2006/2007 at Davis. Spaced antenna (SA) and Doppler beam steering (DBS) experiments were commonly used at all sites for the PMSE observation. To simplify the application of the calibration factor to the data the same experiment configuration was also used for the absolute calibration procedures.

Volume reflectivity was derived from the signal power for several seasons of PMSE observations. The occurrence rates of PMSE were derived from 5-min mean values of radar volume reflectivity. A PMSE event was defined as a radar reflectivity enhancement above the detection limits, but for a minimum duration of 20 min (i.e. 4 consecutive 5-min averages) in one height channel. Finally a mean seasonal data set of volume reflectivity and PMSE occurrence was derived for each site. Figure 6 shows the measurement range of volume reflectivity obtained at Andenes, Davis and Resolute Bay in comparison with data from recent radar observations at other
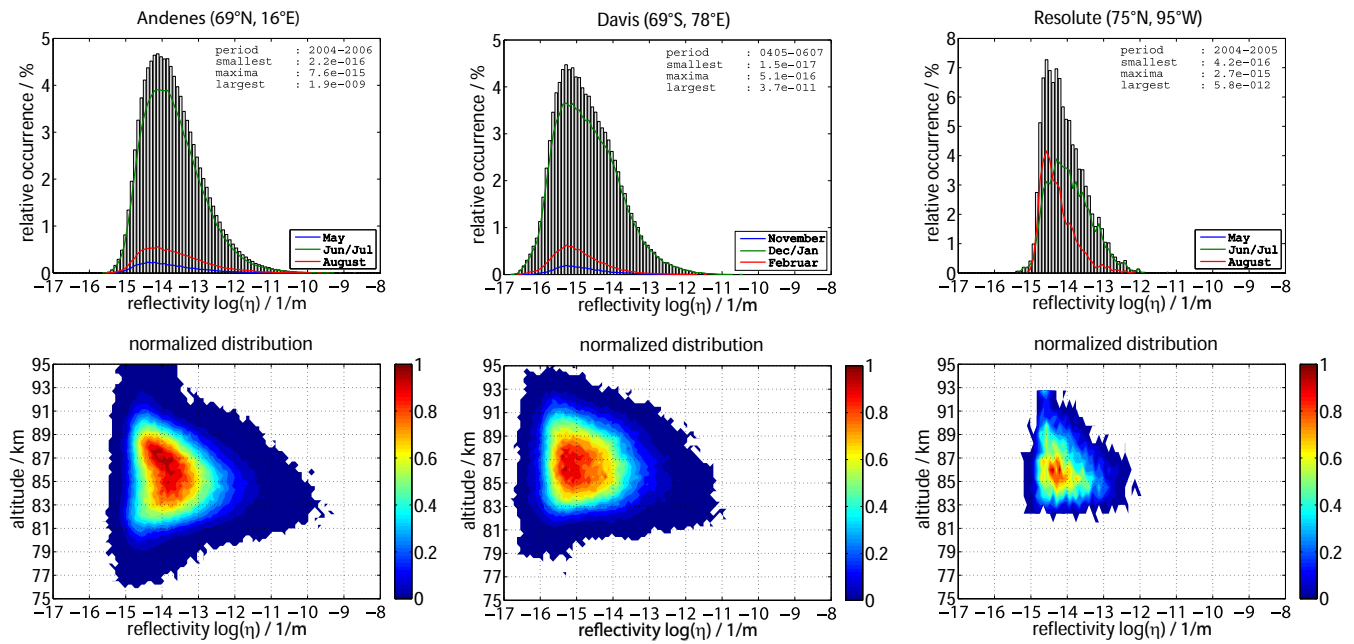
Fig. 7. Relative occurrence of reflectivity and their normalized distribution vs. altitude after PMSE observation at Andenes (2004–2006, left), Davis (0405–0607, middle) and Resolute Bay (2004–2005, right).

Table 2. Minimum detectable and maximum detected volume radar reflectivity during PMSE observations at Andenes, Davis and Resolute Bay.

Radar site	Andenes	Davis	Resolute Bay
Geogra. loc.	69° N, 16° E	69° S; 78° E	75° N; 95° W
Geomag. loc.	67° N, 113° E	76° S; 128° E	83° N; 303° E
Periods	2004–2006	0405–0607	2004–2005
η_{min} [m^{-1}]	2.2×10^{-16}	1.5×10^{-17}	4.2×10^{-16}
η_{max} [m^{-1}]	1.9×10^{-9}	3.7×10^{-11}	5.8×10^{-12}
η_{max}/η_{min}	8.6×10^{6}	2.5×10^{6}	1.3×10^{4}

locations. The relative occurrence of volume reflectivity and their normalized distribution vs. altitude for all three sites is presented in Fig. 7. Minimum and maximum detected volume radar reflectivity for the given periods of PMSE observations are extracted from the mean seasonal data sets and listed in Table 2. Significant differences are given in the sensitivity of the radars mainly caused by the individual experiment configurations used at the three sites as shown in the lower part of Table 1. Especially the product $m \cdot n$ has an important impact on the minimum detection limit of radar volume reflectivity as it improves signal-to-noise ratio of the complete receiving system.

The maximum reflectivity measured at Andenes is about 1.5 orders of magnitude larger than the largest value observed

at Davis indicating that SH-PMSE are weaker than their NH-counterparts at the same geographic latitude. The huge difference in maximum reflectivity observed at Andenes and Resolute Bay of more than 2 orders of magnitude suggests strong longitudinal differences of PMSE characteristics in the Northern Hemisphere. Resolute Bay is located close to the magnetic north pole where particle precipitation influencing the occurrence of PMSE might be different from the particle precipitation at Andenes which is located within the auroral oval most of the time.

The red line in Fig. 6 marks the minimum reflectivity of 1×10^{-15} m^{-1} chosen as a common threshold for the determination of PMSE occurrence rates at Andenes and Davis. The value was close to the detection limit of the Davis VHF radar before the system upgrade in January 2005 as discussed in detail in Latteck et al. (2007).

4.2 Comparison of PMSE observations from Andenes (69° N) and Davis (69° S)

Interhemispheric similarities and dissimilarities of PMSE were studied using occurrence rates based on three years of PMSE observations at Andenes and Davis.

Figure 8 shows the seasonal distribution and variation of PMSE occurrence and their diurnal variation above Andenes and Davis. The occurrence rates refer to radar reflectivities above a common threshold of 1×10^{-15} m^{-1}, and to the number of 5-min averages per day (maximum 288). The seasonal occurrence rate in the middle plots is based on the occurrence
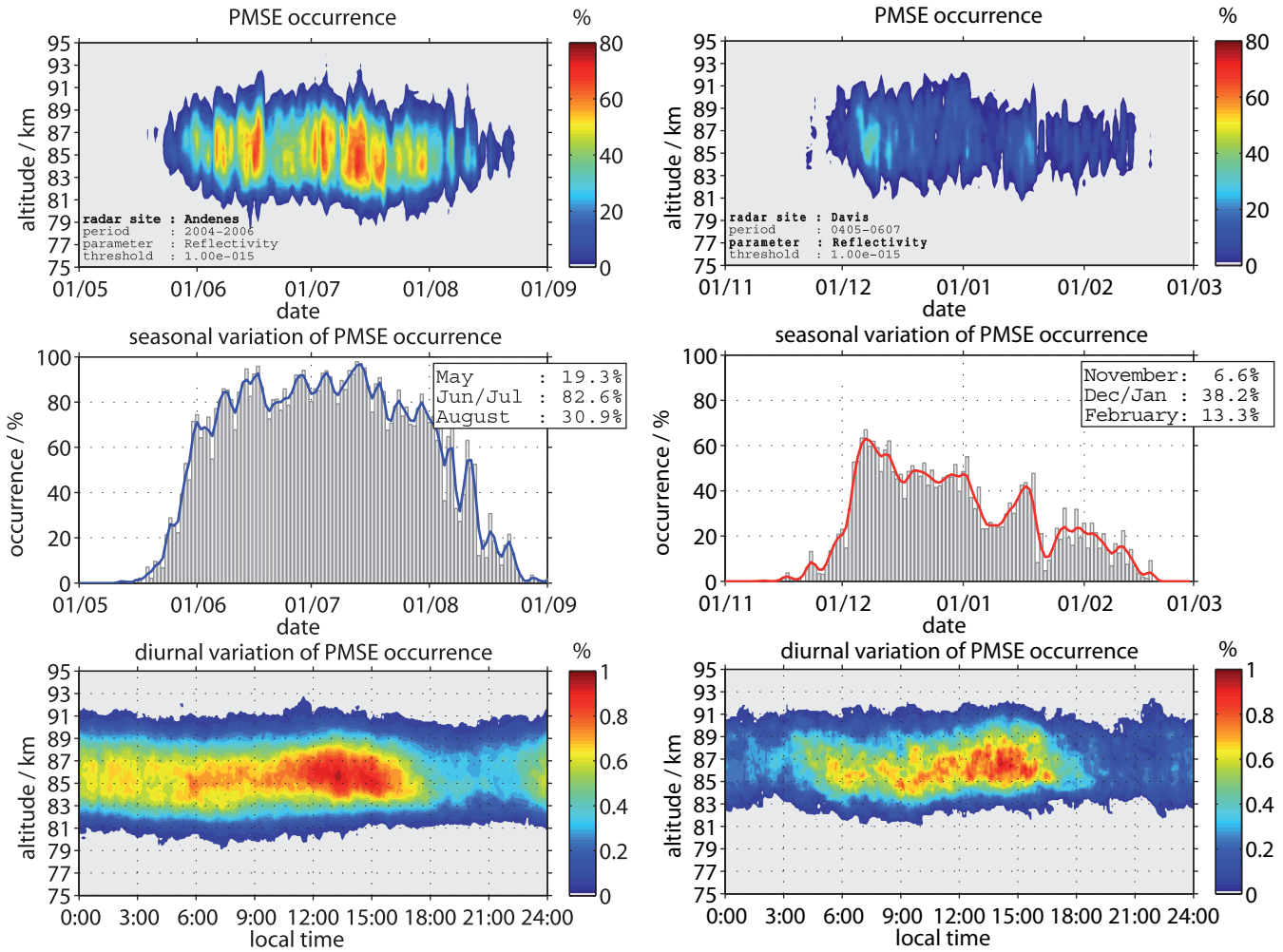
Fig. 8. Seasonal distribution and variation of PMSE occurrence and their diurnal variation above Andenes (2004–2006, left), and Davis (2004/2005–2006/2007, right). The occurrence rates refer to radar reflectivities above a common threshold of 1×10^{-15} m^{-1}, and to the number of 5-min averages per day (maximum 288). The seasonal occurrence rate in the middle plots is based on the occurrence of a PMSE event at any height within a 5-min time bin. The solid lines represent a 3-day running mean value (binominal filter). The bottom plots show the daily occurrence rate of PMSE normalized to its maximum.

of a PMSE event at any height within a 5-min time bin. The bottom plots show the daily occurrence rate of PMSE normalized to its maximum. The mean PMSE occurrence at Andenes reaches a maximum between 11:00–16:00 LT as known from recent observations (e.g. Hoffmann et al., 1999) and has a pronounced minimum at 18:00–22:00 LT. Between 22:00 and 11:00 LT several weaker enhancements in occurrence are observed. A similar behavior was found for the austral summer of 2004/2005 above Davis (Latteck et al., 2007) and this characteristic can be verified by the current study of a mean season of Davis observations. However the minimum occurrence at Davis is not so well pronounced as in the Andenes observations.

The seasonal height distribution and variation of PMSE is presented in the top and middle panels of Fig. 8; a direct comparison of the seasonal variation of PMSE occurrence between Andenes and Davis is shown in Fig. 9. The mean seasonal PMSE occurrence above Davis is lower and has a much greater variability compared to the observations above Andenes. At the beginning of the PMSE season (day −51 to −21 r.t.s.) the monthly mean value of daily occurrence reached 19% at Andenes but only 7% at Davis. During the PMSE core period (day −20 to 40 r.t.s) June/July and December/January, respectively the mean occurrence rate at Davis (38%) is about half the amount as observed at Andenes (83%). The results are summarized in Table 4. The end of the PMSE season at Davis is marked by a sudden
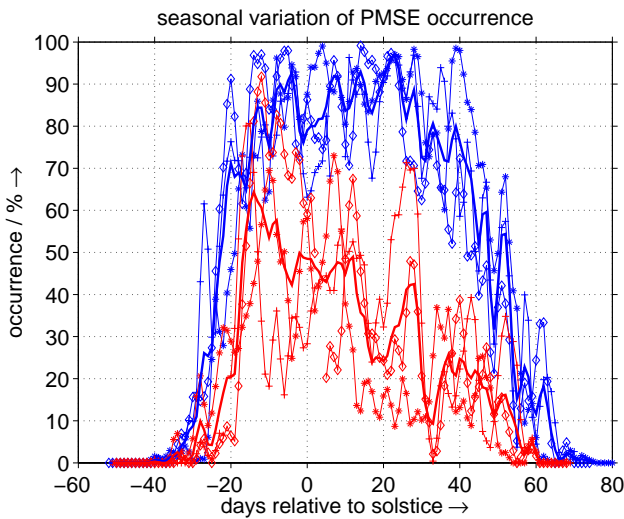
Fig. 9. Seasonal variation of PMSE occurrence above Andenes (2004–2006, blue) and Davis (2004/2005–2006/2007, red) based on radar volume reflectivities $\geq 1 \times 10^{-15}\,\mathrm{m}^{-1}$. The thin lines with symbols represent the individual years: + 2004 (2004/2005), ★ 2005 (2005/2006), and ◇ 2006 (2006/2007).

Table 3. Onset and end of seasonal occurrence of PMSE observed at Andenes and Davis.

Radar site	Year	First PMSE Date	r.t.s.	Last PMSE Date	r.t.s.
Andenes	2004	19 May	−33	30 Aug	70
Andenes	2005	13 May	−39	02 Sep	73
Andenes	2006	14 May	−38	29 Aug	69
mean	2004–2006	15 May	−37	30 Aug	70
Davis	2004/2005	23 Nov	−28	18 Feb	59
Davis	2005/2006	17 Nov	−34	19 Feb	60
Davis	2006/2007	19 Nov	−32	18 Feb	59
mean	2004/05–2006/07	18 Nov	−33	18 Feb	59

drop of occurrence frequency around day 32 r.t.s. followed by a reduction in PMSE occurrence after that time. In February 2005 the Davis radar was upgraded shortly after the day when the PMSE occurrence dropped to zero (Latteck et al., 2007), and the subsequent reduced PMSE occurrence was partly discussed as being caused by the calibration procedure. The observations of the following two seasons at Davis showed the same behavior and in February 2006 the PMSE occurrence dropped to zero exactly at the same day r.t.s. as observed in 2005. This interesting feature is clearly seen in the individual seasonal occurrence rates of the Davis PMSE observations shown in Fig. 9 and confirms the accuracy of the described calibration methods as well as the results presented in Latteck et al. (2007).
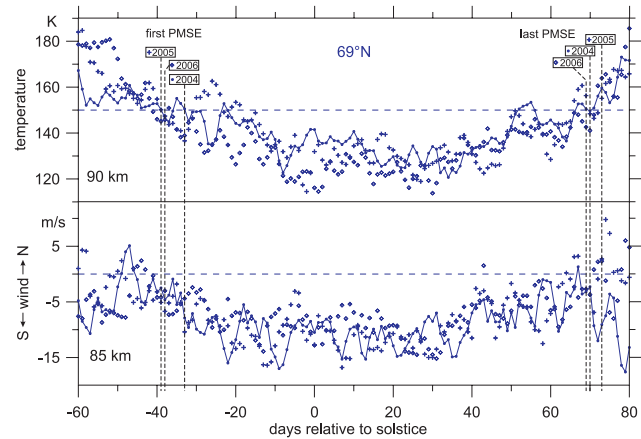

Fig. 10. Daily mean temperatures and mean meridional winds derived from meteor radar observations at Andenes for the summers 2004, 2005, and 2006. The appearance of the first and last PMSE events in these years is indicated by the dashed vertical lines.

Table 3 shows the onset and end of PMSE observed above Andenes and Davis during three periods of observations as well as the averaged mean values. The mean boreal PMSE season above Andenes starts on 15 May and the season ceased on 30 August (days −37 and 70 relative to solstice, r.t.s.). The mean austral season at Davis lasts from 18 November until 18 February (days −33 and 59 r.t.s.) indicating a shorter PMSE season in the SH than in the NH at an equivalent latitude.

The duration of the PMSE season at polar latitudes is highly correlated with the dynamical and thermal state of the mesopause region (Singer et al., 2003; Morris et al., 2007). Figure 10 presents daily mean temperatures around 90 km together with mean meridional winds at 85 km (close to the height of maximum PMSE occurrence) obtained from meteor observations at Andenes (Singer et al., 2003, 2004) during the summer seasons 2004, 2005, and 2006. In general the first PMSE appears if the temperature around 90 km drops below 150 K. The meridional winds are directed towards the equator during this time supporting the transport of PMSE particles from higher latitudes as found by 3-D modelling of the generation of noctilucent cloud particles (Berger and von Zahn, 2007). Mean meridional winds obtained in the Southern Hemisphere at Davis at 86 km in summer 2004/2005 (e.g. Dowdy et al., 2001) are again directed towards the equator in austral summer during the appearance of PMSE. In Fig. 11 these data are shown together with the corresponding meridional winds of the Northern Hemisphere in summer 2004. The occurrence of the first and the last PMSE event are indicated by vertical lines. These observations suggest that PMSE are present at both hemispheres in summer as long as equator ward winds transport cold air from higher to lower latitudes. The shorter SH-occurrence of PMSE is
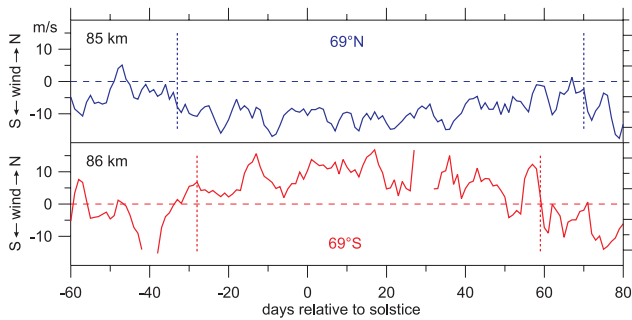
Fig. 11. Daily mean meridional winds obtained from meteor radar observations at Andenes and from MF radar observations at Davis during the boreal summer 2004 and the austral summer 2004/2005. The vertical lines indicate the occurrence of the first and last PMSE.

Fig. 12. Height distribution of PMSE occurrence above Andenes (2004–2006, blue), Davis (0405–0607, red) and Resolute (2004–2005, green) based on radar volume reflectivities $\geq 1 \times 10^{-15}$ m^{-1}.

Table 4. Comparison of mean PMSE occurrences for different periods of the year relative to solstice (r.t.s.) and extreme values of PMSE height distributions at Andenes, Davis and Resolute Bay.

Radar site Periods	Andenes 2004–2006	Davis 0405–0607	Resolute Bay 2004–2005
mean seasonal occurrence rates			
−51 to −21 r.t.s.	19.3%	6.6%	n.a.
−20 to +40 r.t.s.	82.6%	38.2%	18.2%
+41 to +71 r.t.s.	30.9%	13.3%	6.2%
extreme values of height distributions [km]			
$h_{min}(1\%)$	79.8	82.2	83.8
h_{peak}	84.9	85.6	85.2
$h_{max}(1\%)$	91.2	90.6	89.0
$h_{max} - h_{min}$	11.4	8.4	5.2

also reflected in the earlier change of the meridional wind to winter conditions (Dowdy et al., 2001; Morris et al., 2006). The poleward directed winds at Davis around day 50 r.t.s. coincide with a reduced PMSE occurrence above Davis as shown in Fig. 8 and increased temperatures at 85 km between 70° S and 80° S (von Savigny et al., 2007). The earlier end of the PMSE season at Davis around day 60 r.t.s. also coincides with an increase in the mesospheric temperature as measured with falling spheres above Rothera (67° S) in January/February 1998 by Lübken et al. (2004). The observed shorter PMSE season and especially the earlier termination at the Southern Hemisphere was also predicted by Lübken and Berger (2007) using the LIMA/ice model. The model reproduces the main PMSE features as observed by several VHF radars in the NH and SH, respectively. Lübken and Berger (2007) concluded that the NH/SH similarities and differences of PMSE are most likely determined by the thermal structure, whereas other potential reasons, such as turbulence, meteoric smoke particles, ionization, etc., play a minor role.

Figure 12 shows the height distributions of the mean PMSE occurrence rates, the extreme values of the height distributions are summarized in Table 4. The width of the mean PMSE height distribution at 1% is 8.4 km above Davis, about 3 km smaller than at Andenes (11.4 km). The lower height at this point above Davis is 82.2 km, about 2.4 km higher than at Andenes (79.8 km). The top of the extent of the PMSE distribution at both locations is very close together. The maximum of the mean height distribution of PMSE occurrence above Davis occurs at an altitude of 85.6 km, about 0.7 km higher than the maximum of the PMSE height distribution at Andenes (84.9 km); this confirms the results of Latteck et al. (2007) who found a difference in peak altitude of 1 km from a comparison of only one NH and SH PMSE season. A similar difference was found for the peak altitudes of polar mesospheric clouds (PMC). Wrotny and Russell III (2006) analyzed HALOE data obtained between 55° and 70° latitude in both hemispheres and found that the mean altitude
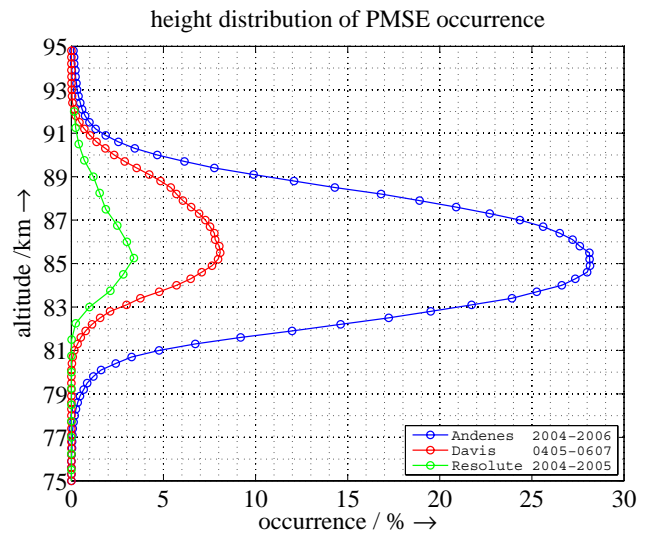
of the SH-PMC distribution is 0.9±0.1 km higher than the mean altitude of the NH-PMC distribution.

4.3 Comparison of PMSE observations from Andenes (69° N, 16° E) and Resolute Bay (75° N, 95° W)

The statistical analysis of the occurrence of PMSE at Resolute Bay is difficult as the radar was not continuously operated for PMSE observation during the summer of 2004 and 2005, especially during July, the main period of PMSE occurrence in the Northern Hemisphere. However, the two late summer periods of PMSE observation at Resolute Bay show generally a lower occurrence rate of about 6% in August compared to 31% at Andenes (Fig. 13, Table 4). The decrease of PMSE occurrence at Resolute Bay started
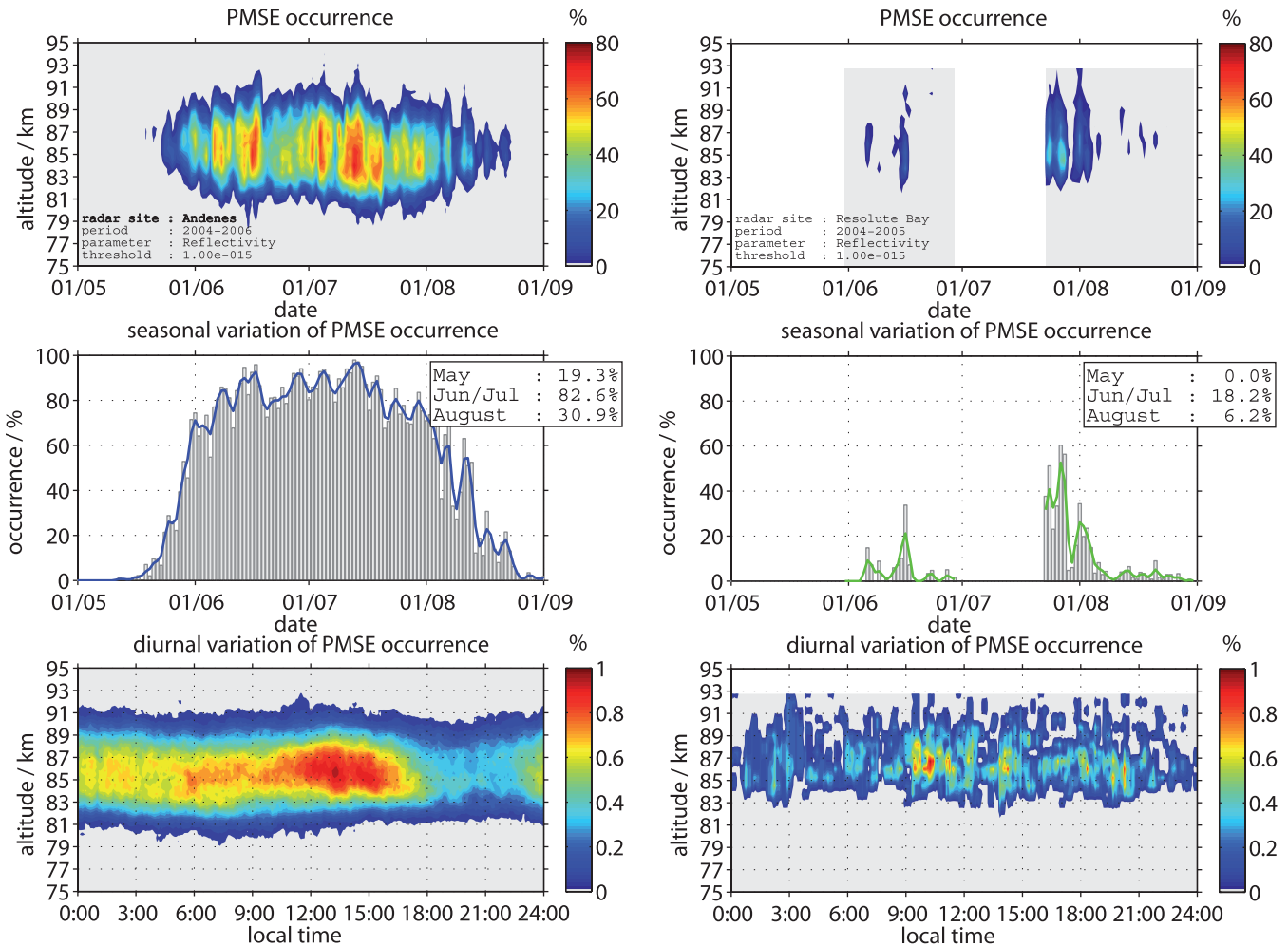
Fig. 13. Seasonal distribution and variation of PMSE occurrence and their diurnal variation above Andenes (2004–2006, left), and Resolute Bay (2004–2005, right). The occurrence rates refer to radar reflectivities above a common threshold of 1×10^{-15} m^{-1}, and to the number of 5-min averages per day (maximum 288). The seasonal occurrence rate in the middle plots is based on the occurrence of a PMSE event at any height within a 5-min time bin. The solid lines represent a 3-day running mean value (binominal filter). The bottom plots show the daily occurrence rate of PMSE normalized to its maximum.

approximately 14 days earlier than at Andenes (Fig. 14) but lasted with only a very few events per day until day 70 r.t.s. which also corresponds to the end of the mean PMSE season at Andenes. From the bottom right plot of Fig. 13 it appears that PMSE occur the whole day over Resolute Bay with a local maximum of occurrence between 09:00 and 12:00 LT. The height distribution (green line in Fig. 12) has a maximum at 85.2 km similar to Andenes, but with very few contributions below 83 km.

The reason for the strong differences in PMSE occurrence between Andenes and Resolute Bay is still unknown. It might be related to the different geomagnetic location of both stations and the connected dependence of PMSE on geomagnetic activity.

5 Conclusions

The comparison of PMSE obtained at different sites requires the calibration of the respective radar systems in order to determine system independent parameters like the radar volume reflectivity. Three VHF radars at Andenes/Norway, Davis/Antarctica and Resolute Bay/Canada were calibrated using the same methods and identical equipment.

The occurrence of PMSE in the Northern and Southern Hemisphere were studied using continuous PMSE observations during the arctic summers of 2004, 2005 and 2006 at Andenes, parts of the arctic summers of 2004 and 2005 at Resolute Bay, and the antarctic summers of 2004/2005, 2005/2006 and 2006/2007 at Davis.
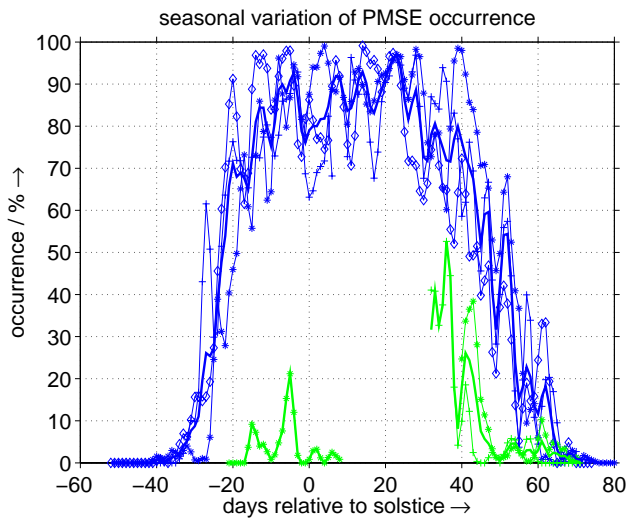
Fig. 14. Seasonal variation of PMSE occurrence above Andenes (2004–2006, blue) and Resolute (2004–2005, green) based on radar volume reflectivities $\geq 1 \times 10^{-15} \, \text{m}^{-1}$. The thin lines with symbols represent the individual years: + 2004, ⋆ 2005, and ⋄ 2006.

The volume reflectivity distribution of PMSE observed at Andenes has a larger maximum ($\sim 2 \times 10^{-9} \, \text{m}^{-1}$) than the distribution of their counterparts observed at Davis ($\sim 4 \times 10^{-11} \, \text{m}^{-1}$). The mean PMSE occurrence is less and more variable above Davis compared to Andenes. The duration of the mean PMSE season at Davis is about 16 days shorter than at Andenes. The diurnal variation of PMSE occurrence has a maximum around 11:00–16:00 LT in both hemispheres. The maximum of the height distribution peaks at 85.5 km at Davis, about 0.7 km higher than the maximum at Andenes. The vertical extent of the mean PMSE height distribution is 8.4 km above Davis, about 3 km smaller than at Andenes. Differences of the mesospheric temperatures are the substantial cause of the observed differences in PMSE occurrence at Davis and Andenes as indicated by model studies and supported by temperature measurements by meteor radars.

The volume reflectivity distribution of PMSE observed at Resolute Bay has a lower maximum ($\sim 6 \times 10^{-12} \, \text{m}^{-1}$) than the distribution of PMSE observed at Andenes. The PMSE occurrence is much lower at Resolute Bay than at Andenes. The decrease of the PMSE season at Resolute Bay starts earlier than at Andenes but the end of the PMSE season is very close at both sites. The PMSE height distribution at Resolute Bay has a maximum at 85 km but with only a few contributions below 83 km. The causes for these strong differences are still not known but might be related to differences in the location of the radars relative to the magnetic north pole and the aurora oval.

References

Balsley, B. B., Woodman, R. F., Sarango, M., Urbina, J., Rodriguez, R., Ragaini, E., and Carey, J.: Southern-hemisphere PMSE: Where are they?, Geophys. Res. Lett., 20, 1983–1985, doi:10.1029/93GL02244, 1993.

Balsley, B. B., Woodman, R., Sarango, M., Rodriguez, R., Urbina, J., Ragaini, E., Carey, J., Huaman, M., and Giraldez, A.: On the lack of southern hemisphere polar mesosphere summer echoes, J. Geophys. Res., 100, 11 685–11 693, doi:10.1029/95JD00510, 1995.

Berger, U. and von Zahn, U.: Three-dimensional modeling of the trajectories of visible noctilucent cloud particles: An indication of particle nucleation well below the mesopause, J. Geophys. Res., 112, doi:10.1029/2006JD008106, 2007.

Cho, J. Y. N. and Röttger, J.: An updated review of polar mesosphere summer echoes: Observation, theory, and their relationship to noctilucent clouds and subvisible aerosols, J. Geophys. Res., 102, 2001–2020, 1997.

Czechowsky, P., Rüster, R., and Schmidt, G.: Variations of mesospheric structures in different seasons, Geophys. Res. Lett., 6, 459–462, 1979.

Dowdy, A., Vincent, R. A., Igarashi, K., Murayama, Y., and Murphy, D. J.: A comparison of mean winds and gravity wave activity in the northern and southern polar MLT, Geophys. Res. Lett., 28, 1475–1478, doi:10.1029/2000GL012576, 2001.

Ecklund, W. L. and Balsley, B. B.: Long-term observations of the Arctic mesosphere with the MST radar at Poker Flat, Alaska, J. Geophys. Res., 86, 7775–7780, 1981.

Green, J. L., Clark, W. L., Warnock, J. M., and Ruth, K. L.: Absolute calibration of MST/ST radars, Preprints, 21st Conference on Radar Meteorology, Edmonton, AB, Am. Meteorol. Soc., pp. 144–147, 1983.

Hocking, W. K.: Measurements of turbulent energy dissipation rates in the middle atmosphere by radar techniques: A review, Radio Sci., 20, 1403–1422, 1985.

Hocking, W. K. and Röttger, J.: Studies of polar mesosphere summer echoes over EISCAT using calibrated signal strengths and statistical parameters, Radio Sci., 32, 1425–1444, 1997.

Hocking, W. K., Kelley, M., Rogers, R., Brown, W. O. J., Moorcroft, D., and St. Maurice, J.-P.: Resolute Bay VHF radar: A multipurpose tool for studies of tropospheric motions, middle atmosphere dynamics, meteor physics, and ionospheric physics, Radio Sci., 36, 1829–1857, doi:10.1029/2000RS001005, 2001.

Hoffmann, P., Singer, W., and Bremer, J.: Mean seasonal and diurnal variations of PMSE and winds from 4 years of radar observations at ALOMAR, Geophys. Res. Lett., 26, 1525–1528, doi:10.1029/1999GL900279, 1999.

Huaman, M. M. and Balsley, B. B.: Differences in near-mesopause summer winds, temperatures, and water vapor at northern and southern latitudes as possible causal factors for inter-hemispheric PMSE differences, Geophys. Res. Lett., 26, 1529–1532, doi:10.1029/1999GL900294, 1999.

Inhester, B., Ulwick, J. C., Cho, J., Kelly, C., and Schmidt, G.: Consistency of rocket and radar electron density observations: implication about the anisotropy of mesospheric turbulence, J. Atmos. Terr. Phys., 52, 855–873, 1990.

Kelley, M. and Ulwick, J.: Large- and small-scale organization of electrons in the high-latitude mesosphere: Implications of the STATE data, J. Geophys. Res., 93, 7001–7008, 1988.

Kelley, M. C., Farley, D. T., and Röttger, J.: The effects of cluster ions on anomalous VHF backscatter from the summer polar mesosphere, Geophys. Res. Lett., 14, 1031–1034, 1987.

Kirkwood, S., Wolf, I., Nilsson, H., Dalin, P., Mikhaylova, D., and Belova, E.: Polar mesosphere summer echoes at Wasa, Antarctica (73° S): First observations and comparison with 68° N, Geophys. Res. Lett., L15803, doi:10.1029/2007GL030516, 2007.

Latteck, R., Singer, W., and Bardey, H.: The ALWIN MST radar – Technical design and performances, in: Proceedings of the 14th ESA Symposium on European Rocket and Balloon Programmes and Related Research, Potsdam, Germany (ESA SP–437), edited by: Kaldeich-Schürmann, B., pp. 179–184, 1999.

Latteck, R., Singer, W., Morris, R. J., Holdsworth, D. A., and Murphy, D. J.: Observation of polar mesosphere summer echoes with calibrated VHF radars at (69° N) in the Northern and Southern Hemispheres, Geophys. Res. Lett., 34, L14805, doi:10.1029/2007GL030032, 2007.

Lübken, F.-J. and Berger, U.: Interhemispheric comparison of mesospheric ice layers from the LIMA model, J. Atmos. Solar Terr. Phys., 69(17–18), 2292–2308, doi:10.1016/j.jastp.2007.07.006, 2007.

Lübken, F.-J., Jarvis, M. J., and Jones, G. O. L.: First in situ temperature measurements at the Antarctic summer mesopause, Geophys. Res. Lett., 26, 3581–3584, doi:10.1029/1999GL010719, 1999.

Lübken, F.-J., Müllemann, A., and Jarvis, M. J.: Temperatures and horizontal winds in the Antarctic summer mesosphere, J. Geophys. Res., 109, D24112, doi:10.1029/2004JD005133, 2004.

Morris, R. J., Murphy, D. J., Reid, I. M., Holdsworth, D. A., and Vincent, R. A.: First polar mesosphere summer echoes observed at Davis, Antarctica (68° S), Geophys. Res. Lett., 31, L16111, doi:10.1029/2004GL020352, 2004.

Morris, R. J., Murphy, D. J., Vincent, R. A., Holdsworth, D. A., Klekociuk, A. R., and Reid, I. M.: Characteristics of the wind, temperature and PMSE field above Davis, Antarctica, J. Atmos. Solar Terr. Phys., 68, 418–435, doi:10.1016/j.jastp.2005.04.011, 2006.

Morris, R. J., Murphy, D. J., Klekociuk, A. R., and Holdsworth, D. A.: First complete season of PMSE observations above Davis, Antarctica, and their relation to winds and temperatures, Geophys. Res. Lett., 34, L05805, doi:10.1029/2006GL028641, 2007.

Probert-Jones, J. R.: The Radar Equation in Meteorology, Q. J. Roy. Meteorol. Soc., 88, 485–495, 1962.

Rapp, M. and Lübken, F.-J.: Polar mesosphere summer echoes (PMSE): Review of observations and current understanding, Atmos. Chem. Phys., 4, 2601–2633, 2004, http://www.atmos-chem-phys.net/4/2601/2004/.

Singer, W., Bremer, J., Hocking, W., Weiß, J., Latteck, R., and Zecha, M.: Temperature and wind tides around the summer mesopause at middle and arctic latitudes, Adv. Space Res., 31, 2055–2060, doi:10.1016/S0273-1177(03)00228-X, 2003.

Singer, W., Bremer, J., Weiß, J., Hocking, W., Höffner, J., Donner, M., and Espy, P.: Meteor radar observations at middle and arctic latitudes – Part 1: Mean temperatures, J. Atmos. Solar Terr. Phys., 66, 607–616, doi:10.1016/j.jastp.2004.01.012, 2004.

Skolnik, M.: Radar handbook, McGraw-Hill, p. 2.27, 1990.

Stebel, K., Blum, U., Fricke, K.-H., Kirkwood, S., Mitchell, N., and Osepian, A.: Joint radar/lidar observations of possible aerosol layers in the winter mesosphere, J. Atmos. Solar Terr. Phys., 66, 957–970, doi:10.1016/j.jastp.2004.03.008, 2004.

von Savigny, C., Sinnhuber, M., Bovensmann, H., Burrows, J. P., Kallenrode, M.-B., and Schwartz, M.: On the disappearance of noctilucent clouds during the January 2005 solar proton events, Geophys. Res. Lett., 34, L02805, doi:doi:10.1029/2006GL028106, 2007.

Woodman, R. F., Balsley, B. B., Aquino, F., Flores, L., Vazquez, E., Sarango, M., Huamann, M. M., and Soldi, H.: First observations of polar mesosphere summer echoes in Antarctica, J. Geophys. Res., 104, 22 577–22 590, doi:10.1029/1999JA900226, 1999.

Wrotny, J. E. and Russell III, J. M.: Interhemispheric differences in polar mesospheric clouds observed by the HALOE instrument, J. Atmos. Solar Terr. Phys., 68, 1352–1369, doi:10.1016/j.jastp.2006.05.014, 2006.